NREL/TP-442-5623 • UC Category: 261 • DE93010042

Inflow Characteristics Associated with High Blade Loading Events in a Wind Farm

Neil D. Kelley

Prepared for the
IEA Experts Meeting 25
Increased Loads in Wind Power Stations
May 3–4, 1993
Gothenburg, Sweden

National Renewable Energy Laboratory
1617 Cole Boulevard
Golden, Colorado 80401-3393
Operated by Midwest Research Institute
for the U.S. Department of Energy
under Contract No. DE-AC02-83CH10093

Prepared under Task No. WE318010

July 1993

NOTICE

Printed in the United States of America
Available from:
National Technical Information Service
U.S. Department of Commerce
5285 Port Royal Road
Springfield, VA 22161

Price: Microfiche A01
Printed Copy A03

Codes are used for pricing all publications. The code is determined by the number of pages in the publication. Information pertaining to the pricing codes can be found in the current issue of the following publications which are generally available in most libraries: *Energy Research Abstracts (ERA)*; *Government Reports Announcements and Index (GRA and I); Scientific and Technical Abstract Reports (STAR)*; and publication NTIS-PR-360 available from NTIS at the above address.

Printed on recycled paper

IEA Annex XI
Expert Meeting 25, *Increased Loads in Wind Power Stations,, "Wind Farms"*
Gothenburg, May 3-4, 1993

INFLOW CHARACTERISTICS ASSOCIATED WITH HIGH-BLADE-LOADING EVENTS IN A WIND FARM

N.D. Kelley
Wind Technology Division
National Renewable Energy Laboratory
Golden, Colorado U.S.A.

Introduction

The stochastic characteristics of the turbulent inflow have been shown to be of major significance in the accumulation of fatigue in wind turbines. Because most of the wind turbine installations in the United States have taken place in multi-turbine or wind farm configurations, the fatigue damage associated with the higher turbulence levels within such arrangements must be taken into account when making estimates of component service lifetimes. The simultaneous monitoring of two adjacent wind turbines over a wide range of turbulent inflow conditions has given us more confidence in describing the structural load distributions that can be expected in such an environment.

The adjacent testing of the two turbines allowed us to postulate that observed similarities in the response dynamics and load distributions could be considered "quasi-universal," while the dissimilarities could be considered to result from the differing design of the rotors. The format has also allowed us to begin to define appropriate statistical load distribution models for many of the critical components in which fatigue is a major driver of the design. In addition to the adjacent turbine measurements, we also briefly discuss load distributions measured on a teetered-hub turbine.

Approach

Two adjacent Micon 65/13 turbines, installed in a very large wind farm in San Gorgonio Pass, California, were used for the measurements. These rigid-hub turbines were identical except for the rotor blades. The rotor of one turbine consisted of blades based on the NREL (SERI) thin-airfoil family, and the other had refurbished, original-equipment AeroStar blades. Each turbine was extensively instrumented. A wide range of turbine dynamics was rainflow counted. A total of 67.5 hours of operational data over a wide range of inflow conditions is available for analysis from the two Micons. Figure 1 summarizes the distributions of the mean wind speed, wind-speed standard deviation, turbulence intensity, and time of day for the 405, 10-minute records available. A total of 70.1 hours of similar data is available for limited comparison from the prototype NPS100 turbine that incorporated a two-bladed, teetered rotor.

Statistical Load Distribution Models

Our analysis has shown that all of the alternating (range or peak-to-peak) load distributions, can be described using a *mixture of three statistical models*. While the first and second models in the mixture

appear to be well defined by the Gaussian and lognormal distributions, respectively, the third appears to be a function of the turbine dynamic being described. Figure 2 schematically describes the linear summation of the individual model distributions. The p-p root flapwise bending moment distribution is pictured in Figure 3 with each of the contributions to the mixture highlighted. We hypothesize that the three-distribution mixture is a direct result of a similar mixture describing the cyclic content of the wind. The cyclic distributions of the hub-elevation horizontal and vertical wind speeds are plotted in Figure 4. We believe that the infrequent or low-cycle, high-amplitude loads seen by the wind turbines are a consequence of the non-Gaussian characteristics of the turbulent inflow. These are indicated by the shaded areas of Figure 4.

Comparisons of Turbine Dynamic Load Distributions

We present graphic comparisons of the mixed process, cyclic load distributions associated with several turbine dynamics measured on each of the machines under test. Figure 5 plots the summary of observed range or p-p cycles of the root flapwise and edgewise bending moments for the three blades on each turbine. While the flapwise loads are nearly identical, the edgewise loads reflect the greater mass of the AeroStar blades. The low-speed shaft bending and torque distributions are displayed in Figure 6. Again, while the bending distributions are the same, the greater weight of the AeroStar blades appears to be responsible for the higher loading cycles in the high- and mid-frequency cycle range. Figure 7 plots the distributions associated with axial and inplane components of the thrust vector. The NREL rotor exhibits slightly higher low-cycle range axial loads while the AeroStar-equipped rotor displays the same for the inplane component. We believe that the former is a result of a greater swept area and the greater mass of the latter. The identical yaw drive torque distributions are plotted in Figure 8. These results suggest that, when variations in inertia and swept areas are considered, the underlying statistical distributions are identical for both turbines. Also, the striking similarity between the mid- and low-frequency range gust distributions of Figure 4 and the turbine dynamic distributions of Figures 5 through 8 suggests that the latter are the result of the former.

Cycle Counting of Rigid- and Teetered-Hub Turbines

Recently, we compared the sample populations of cyclic load distributions of the flap and edgewise root bending moments from the two rigid-hub Micons and the teetered NPS100 prototype. It was fortunate that the size and weight of the rotor blades for these turbines were similar. A total of 67.5 hours of data in 10-minute records is available for the Micons, and 70.1 hours in 11-minute records is available for the NPS100. The Micon records were rainflow counted individually and as a single record. This process confirmed that, for the flapwise loads, the important low-cycle, high-amplitude range above 15 kNm can be described by an *exponential distribution*. While further work is needed for confirmation, the edgewise loads appear to be more appropriately fitted by an *extreme value distribution* (Type I). Figure 9 plots the flapwise load distributions for the Micons and the NPS100. A decaying exponential has been fitted to each above 15 kNm. This diagram suggests that the teetered hub provides load relief over the rigid hub in the mid-frequency cycle range. It also indicates that little, if any, relief is gained from the most damaging infrequent or low-cycle, high-amplitude excursions.

This leads us to hypothesize an overall model for the statistical load structure as a result of turbulence excitation on wind turbines. Figure 10 schematically describes this hypothesis. We suggest that the overall statistical distribution is a summation of at least four component processes. These components include a high-cycle, low-amplitude Gaussian distribution; what we believe to be a *transition* lognormal distribution; a parameter-dependent low-cycle, high-amplitude distribution; and some form of a *rare* event distribution. The last two are of the most concern. We believe that the low-cycle, high-load range

(about once per operating hour to one in 10,000 hours) results from encountering *coherent turbulent structures* in the turbine inflow and is responsible for a major portion of component fatigue damage. The rare event distribution is primarily related to matters of turbine survivability as a result of violent atmospheric phenomena such as hurricanes, tornadoes, etc., that may occur during the machine's lifetime.

Coherent turbulence load excitation

We analyzed the 405, 10-minute records available from the two Micons and identified the peak loading events [both positive (tension) and negative (compression) peaks], which, when paired, formed the 25 largest and most damaging fatigue cycles. We found the following:

- ***All** of the tension peaks associated with the largest stress cycles occurred during slightly stable flows emerging from a deep canyon southwest of the wind park.*
- *The most common time of occurrence was 22 h local standard time.*
- *The negative (compression) peaks of these cycles occurred during **slightly more stable** conditions centered near 04 h.*

The previous year, we made extensive turbulence measurements up- and downwind of the large wind farm in the San Gorgonio, California, wind farm in which the Micons were located. These measurements indicated that a minimum of at least *three distinct flow regimes* are present in the turbine inflows. The regimes appear to be the result of circulations derived from the surrrounding complex terrain features, transient induced shears resulting from nonlinear atmospheric phenomena such as waves, and (within the wind farm) decaying wakes from upstream turbines. The characteristic times for each are 300, 10, and 1 seconds, respectively. We used the data collected to develop empirical models of three component velocity spectra, spatial coherence, and local cross-axis correlations. As an example, Figure 11 compares the 12 m/s spectra of the crosswind (v) component for unstable, near-neutral, and stable flow conditions up- and downwind of the wind farm and over homogeneous or smooth terrain.

In Figure 12, we present an example of the NREL-equipped rotor meeting a coherent turbulent structure. This encounter produced the largest positive (tension) flapwise moment seen in the Micon 65 data set on this turbine. From the figure, one can see the interaction of each blade with the structure over about a 2-second period. The plots show that Blade No. 3 receives the largest transient tension load while, at the same time, the other two are undergoing compression. This suggests that the entire rotor was concurrently involved. The associated hub-elevation, estimated vorticity/helicity time series has been aligned with the peak on Blade No.3 and is plotted in Figure 13. It also covers a period of about 2 seconds, suggesting a strong correlation of the two events.

Conclusions

There is significant evidence that the largest loads in the low-cycle frequency range are produced by the rotor interacting with a coherent turbulent structure. These interactions produced a coherent (phase specific) response in the turbine's rotor and other components as a result of the simultaneous excitement of multiple structural modes. The period of these excursions (at least in the root flapwise bending

moment) is much less than the period of one rotor revolution. The most damaging tension peaks occur during atmospheric conditions likely to support wave motions and extended wakes.

Acknowledgement

This work has been supported by the U.S. Department of Energy under contract DE-AC02-83CH10093.

References

Kelley, N.D., "Full Vector (3-D) Inflow Simulation in Natural and Wind Farm Environments Using an Expanded Version of the SNLWIND (Veers) Turbulence Code," NREL TP-442-5225, National Renewable Energy Laboratory, November 1992.

Olesen, H.R., S.E. Larsen, and J. Højstrup, "Modeling Velocity Spectra in the Lower Part of the Planetary Boundary Layer," *Boundary-Layer Meteorology*, Vol. 29, 1984.

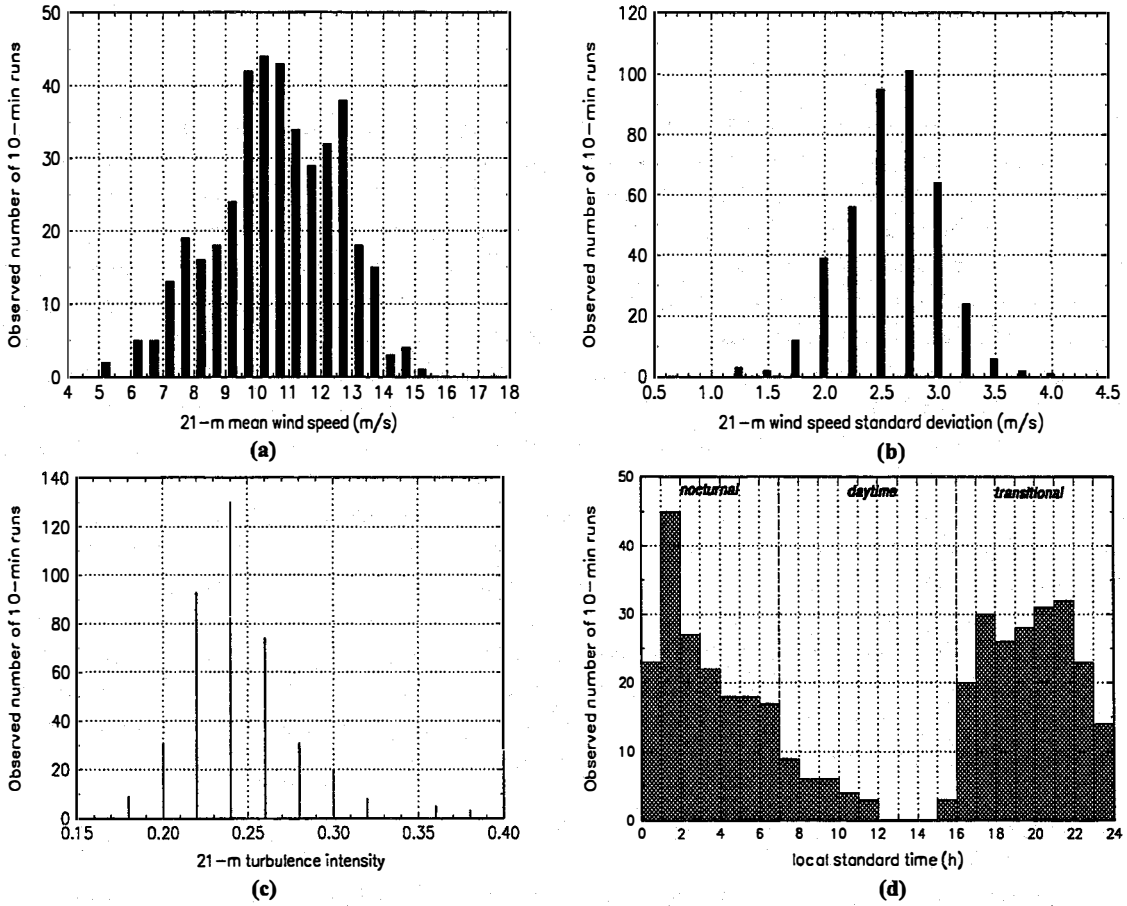

Figure 1. Histogram summaries at 21m: (a) mean wind speed, (b) wind-speed standard deviation, (c) turbulence intensity, and (d) time of day for the 405 data records used in the Micon 65 study

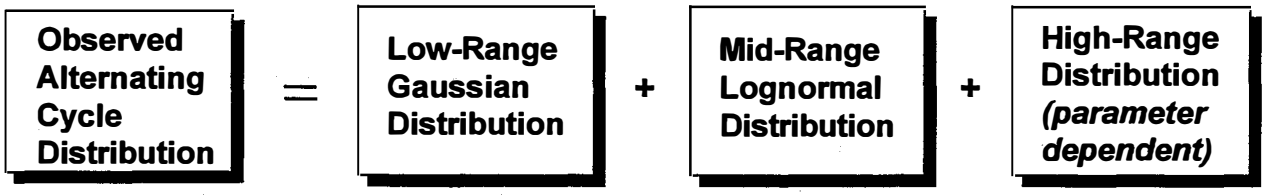

Figure 2. Suggested components of a mixed distribution model to explain observed alternating loads

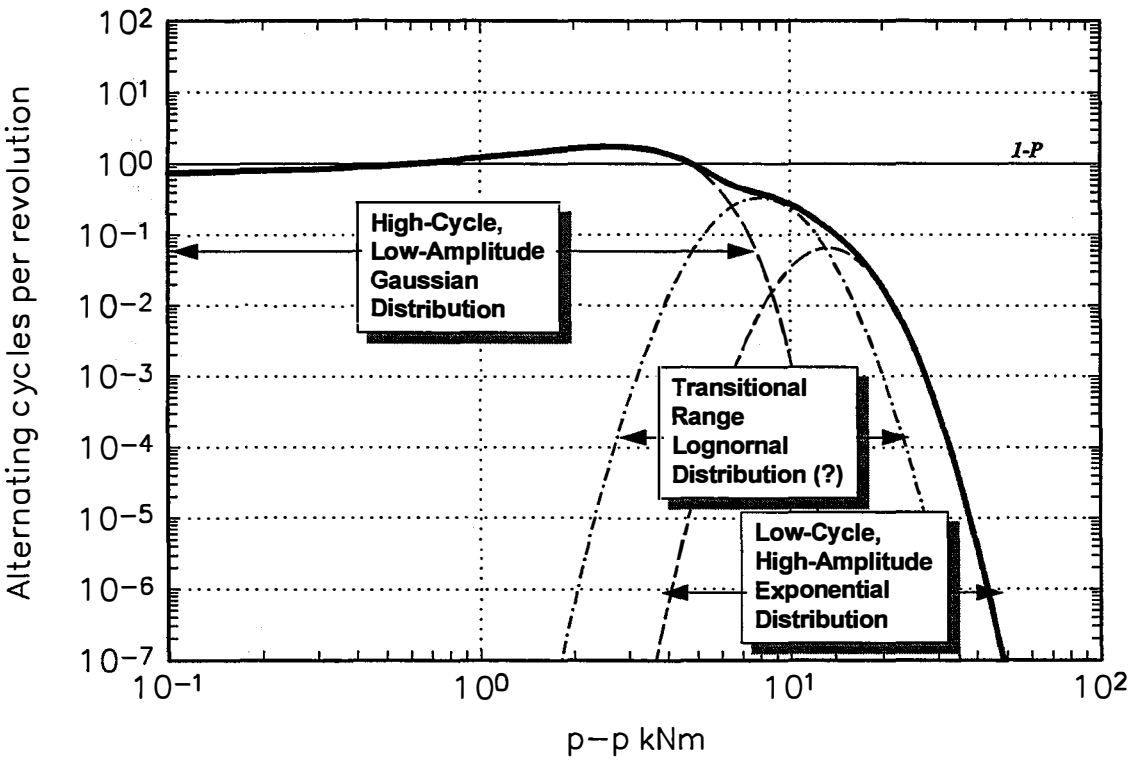

Figure 3. An example of the the mixed distribution model for the p-p root flapwise bending

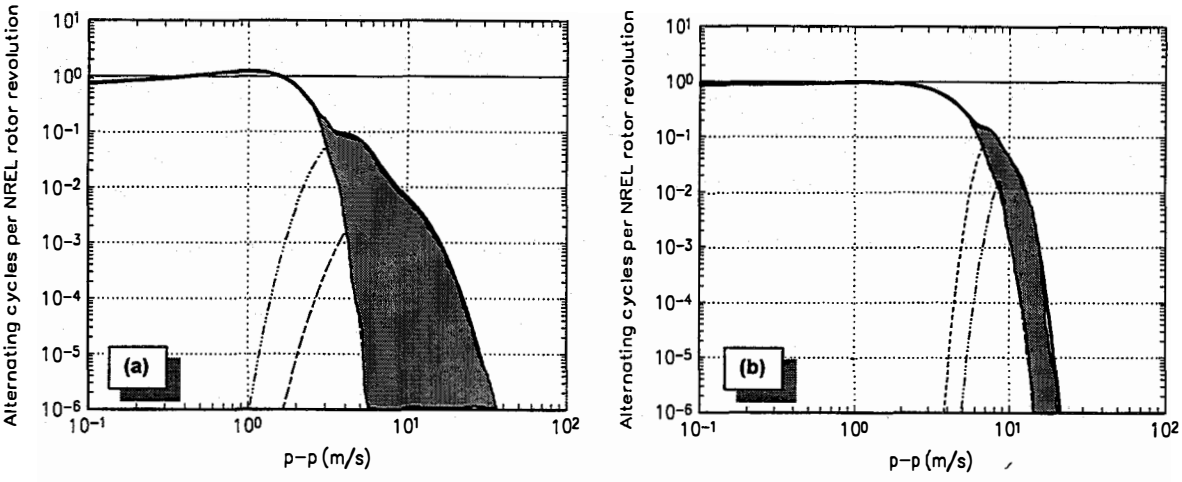

Figure 4. Observed wind speed component alternating cycle distributions: (a) horizontal wind speed (b) vertical wind speed

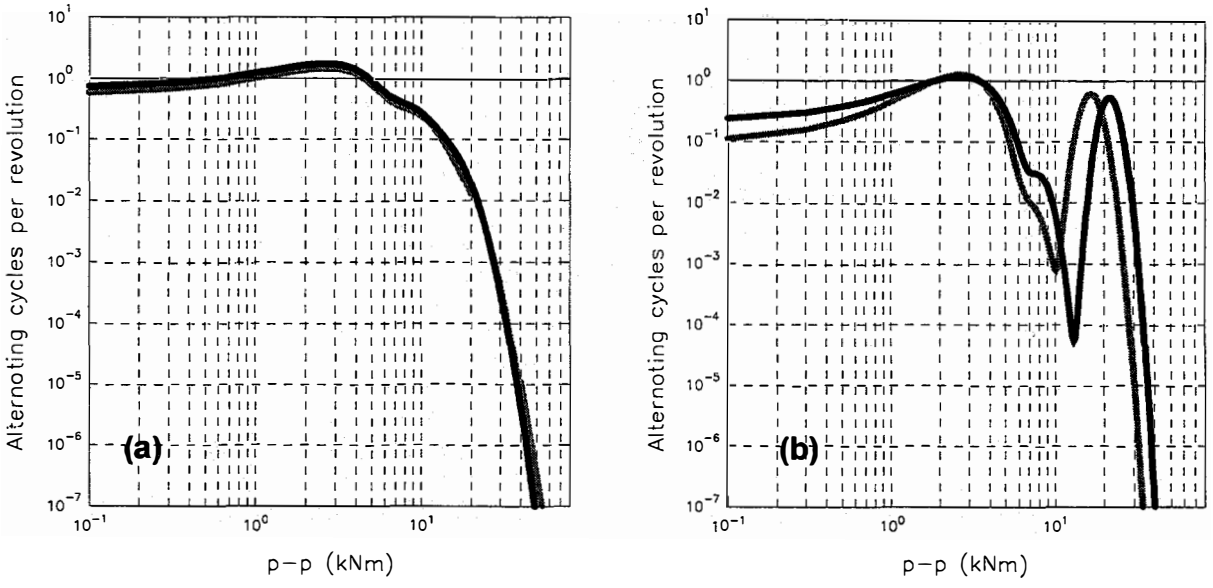

Figure 5. Three-blade flapwise (a) and edgewise (b) root bending alternating cycle distributions

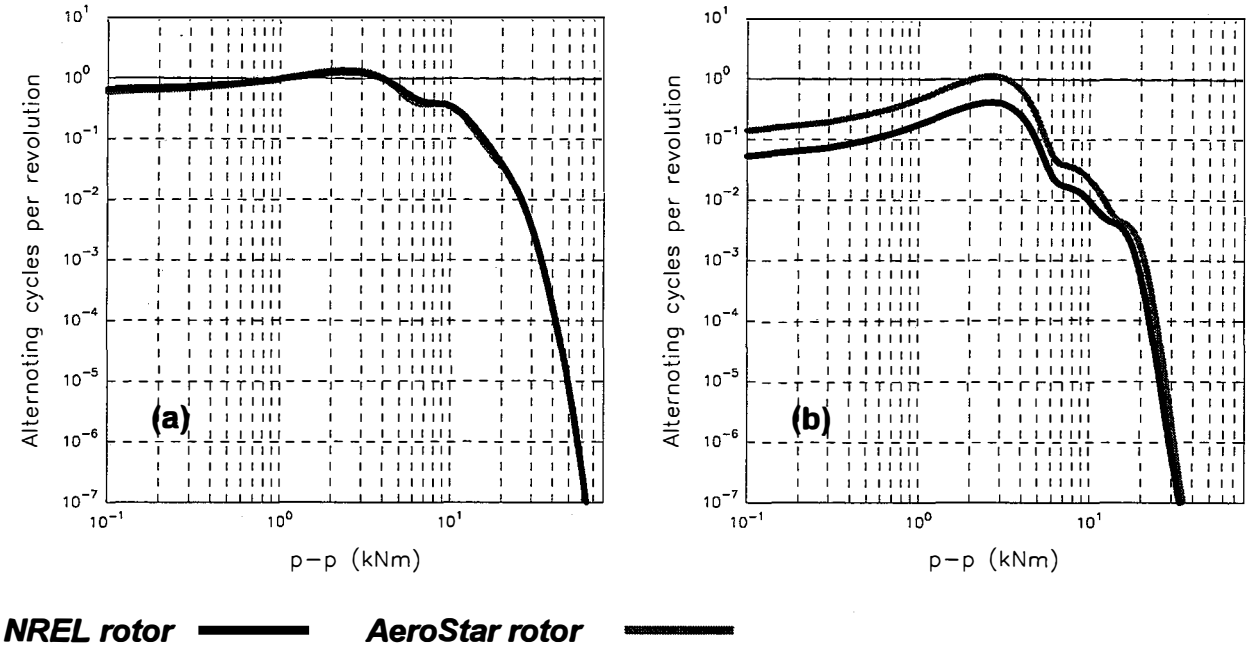

Figure 6. Low-speed shaft bending (a) and torque (b) cyclic distributions

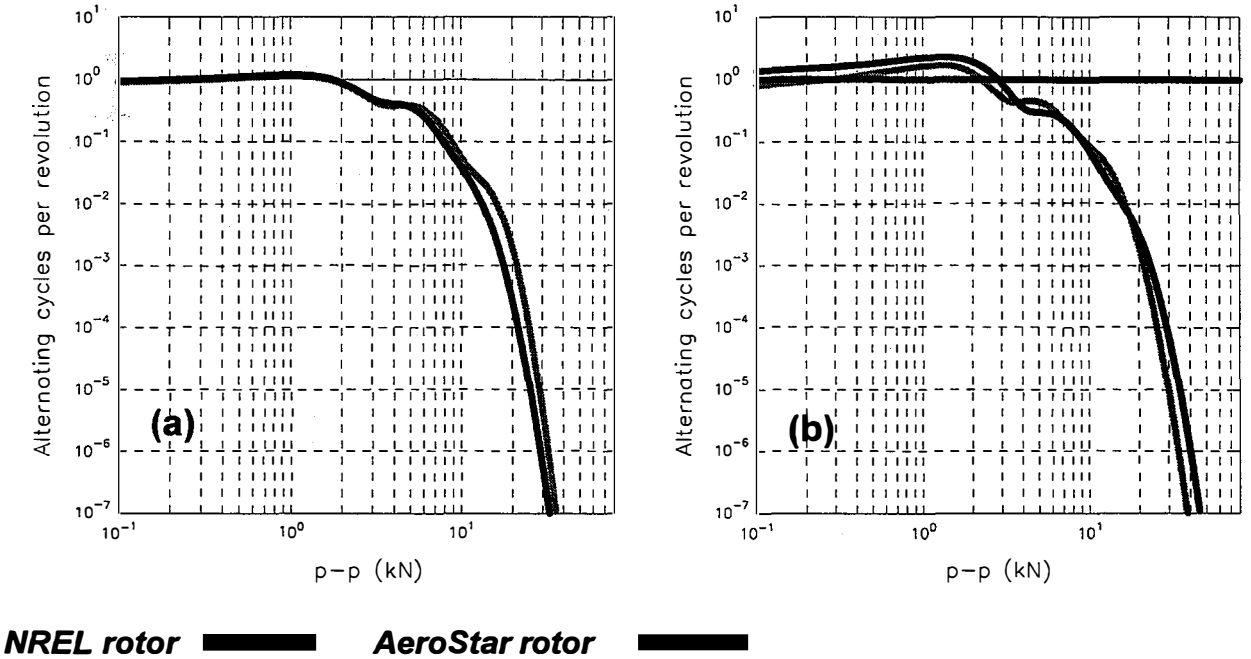

Figure 7. Axial (a) and inplane (b) thrust component cyclic distributions

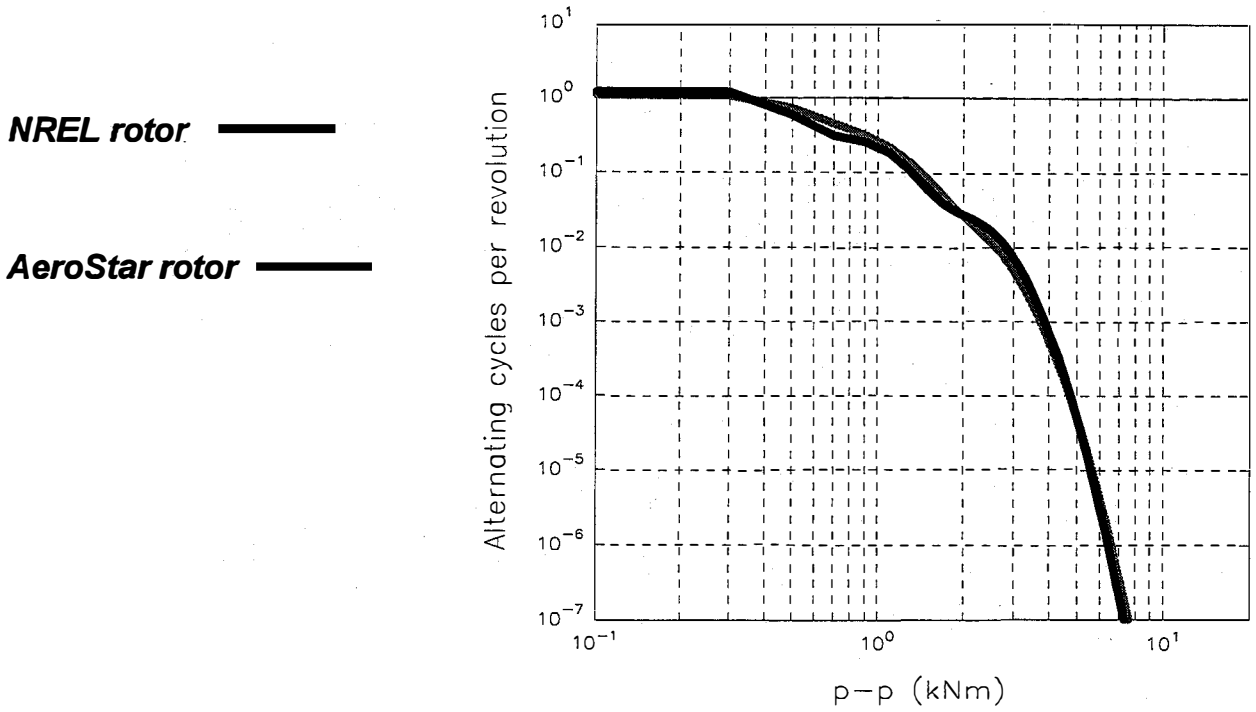

Figure 8. Yaw drive torque cyclic distributions

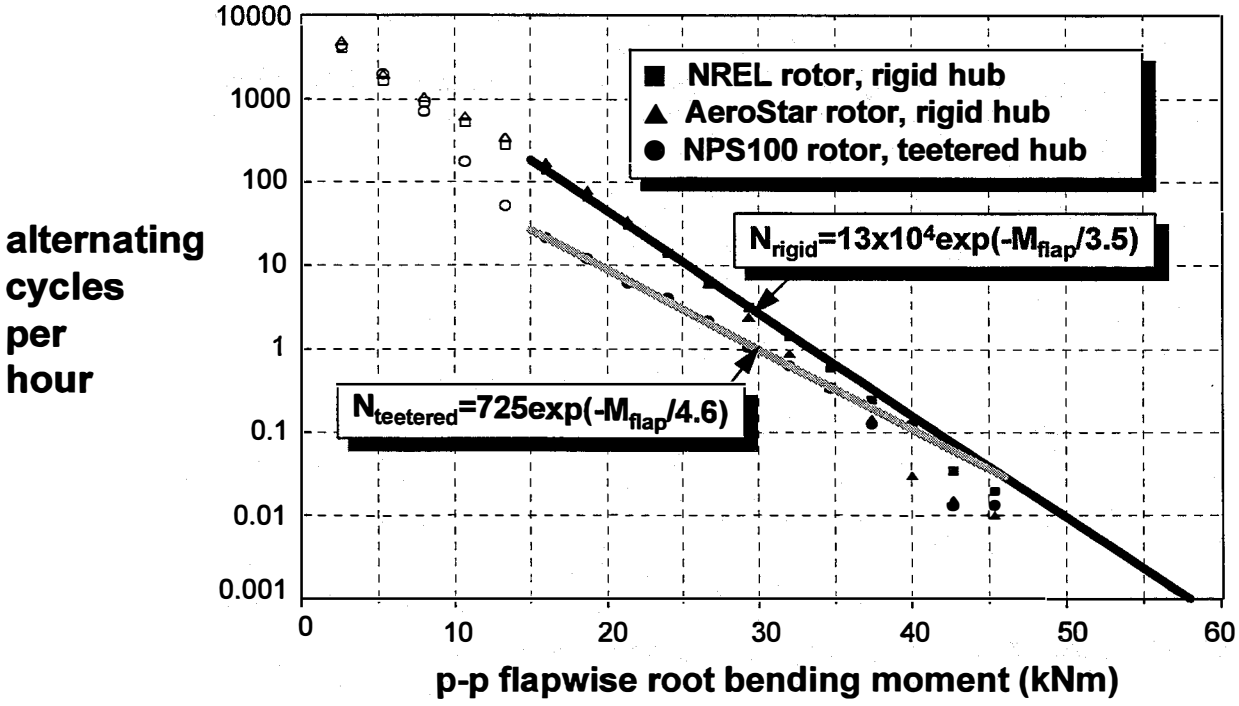

Figure 9. Comparison of rigid- versus teetered-hub low-cycle alternating flapwise loads

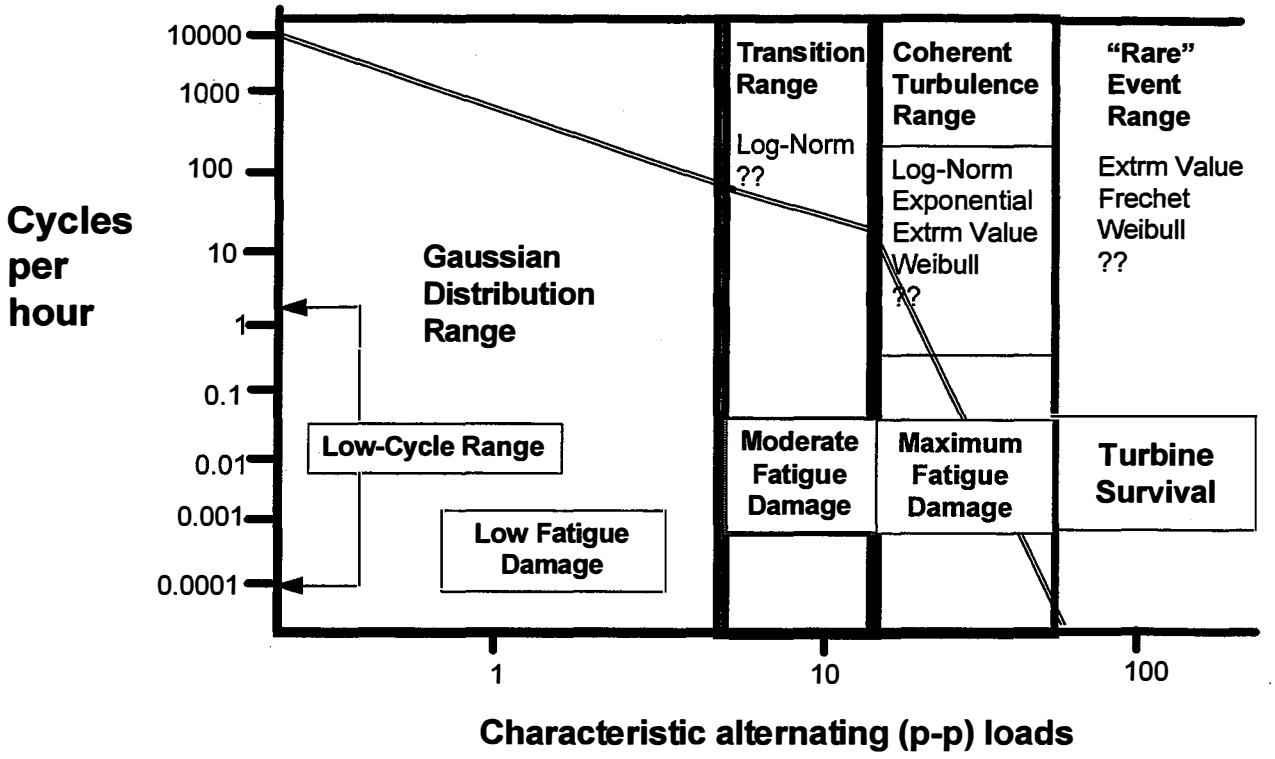

Figure 10. Hypothesized turbulence-loading statistical structure

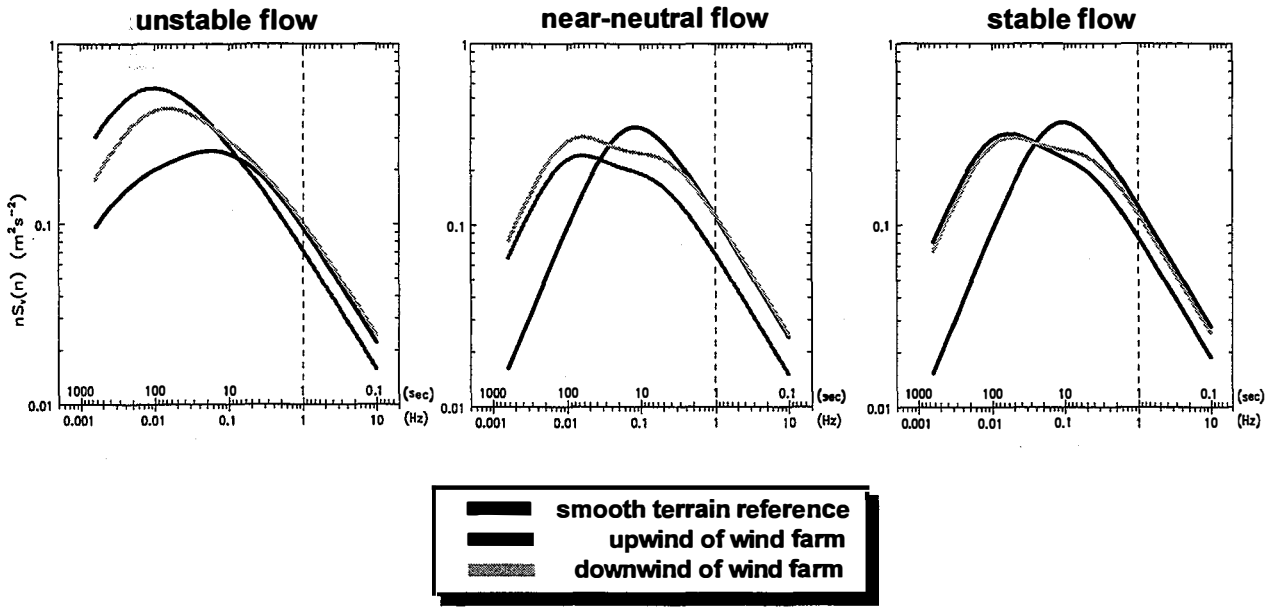

Figure 11. Comparison of predicted crosswind (v) velocity spectra for 12 m/s mean wind speed

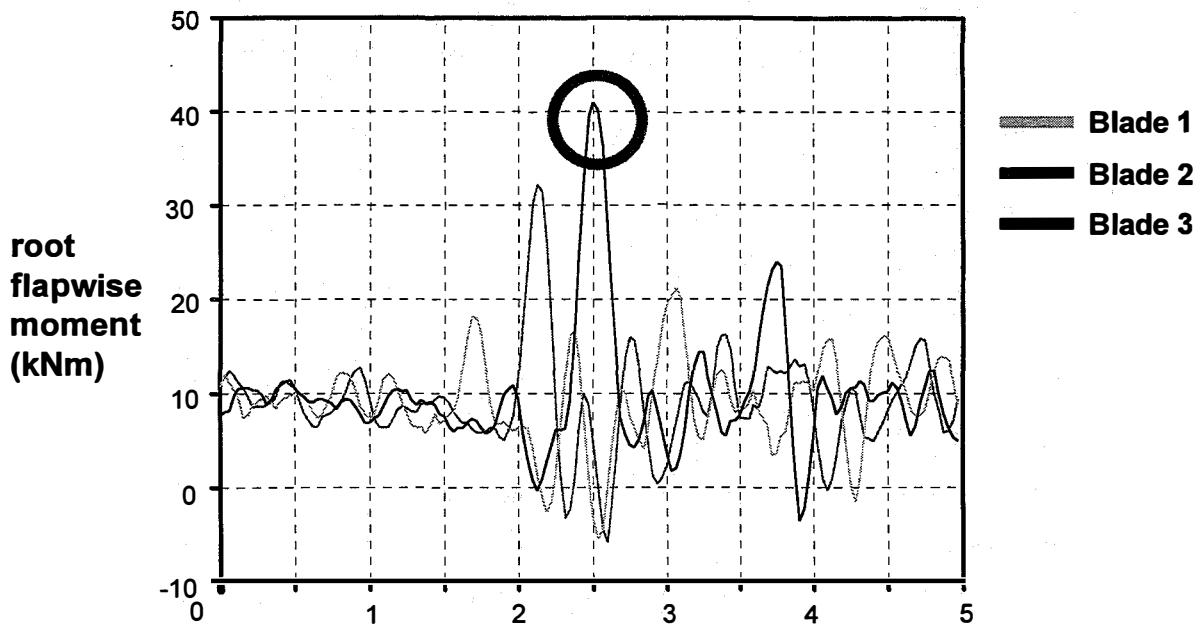

Figure 12. Largest positive (tension) peak stress cycle observed for the NREL rotor

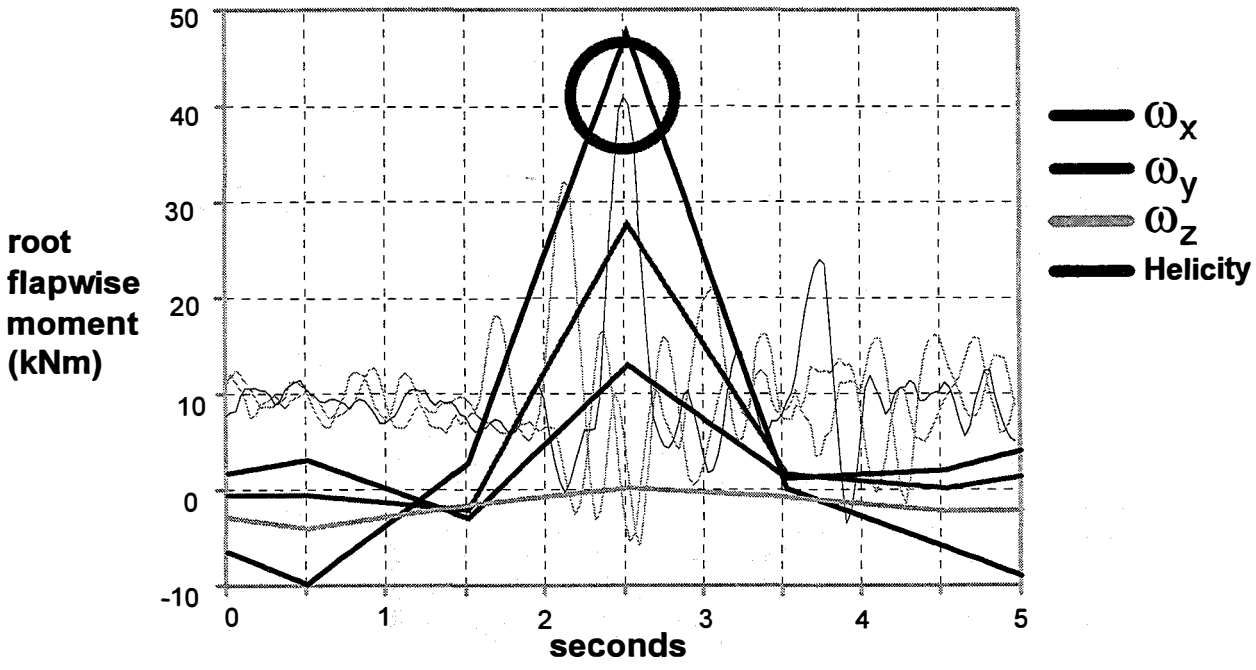

Figure 13. Hub-height vorticity/helicity estimates aligned with peak flapwise moment